Title

Heart Rate-Independent 3D Myocardial Blood Oxygen Level-Dependent MRI at 3.0 T with Simultaneous 13N-Ammonia PET Validation.

Journal

Radiology, 295(1)

ISSN

0033-8419

Authors

Yang, Hsin-Jung
Dey, Damini
Sykes, Jane
et al.

Publication Date

2020-04-01

DOI

10.1148/radiol.2020191456

Peer reviewed

Radiology

Heart Rate–Independent 3D Myocardial Blood Oxygen Level–Dependent MRI at 3.0 T with Simultaneous ^{13}N–Ammonia PET Validation

Hsin-Jung Yang, PhD • Damini Dey, PhD • Jane Sykes, BS • John Butler, BS • Heather Biernaski, BS • Michael Kovacs, PhD • Xiaoming Bi, PhD • Behzad Sharif, PhD • Ivan Cokic, MD • Richard Tang, MD • Piotr Slomka, PhD • Frank S. Prato, PhD • Rohan Dharmakumar, PhD

From the Department of Biomedical Sciences, Cedars-Sinai Medical Center, Biomedical Imaging Research Institute, PACT Bldg–Suite 400, 8700 Beverly Blvd, Los Angeles, CA 90048 (H.J.Y., D.D., B.S., I.C., R.T., P.S., R.D.); Department of Bioengineering (H.J.Y., R.D.) and David Geffen School of Medicine (D.D., P.S.), University of California, Los Angeles Calif; Lawson Health Research Institute, London, Canada (J.S., J.B., H.B., M.K., F.S.P.); and MR R&D, Siemens Healthcare, Los Angeles, Calif (X.B.). Received July 3, 2019; revision requested August 14; revision received December 20; accepted January 3, 2020. **Address correspondence to** H.J.Y. (e-mail: *Hsin-Jung.Yang@cshs.org*).

R.D. supported by a grant from the National Institutes of Health (NIH/R01 HL091989); F.S.P. supported by a grant from Ontario Research Fund (ORF RS7-021) and Canada Foundation for Innovation (CFI#11358).

Conflicts of interest are listed at the end of this article.

See also the editorial by Almeida in this issue.

Radiology 2020; 295:82–93 • https://doi.org/10.1148/radiol.2020191456 • Content codes: CA MR

Background: Despite advances, blood oxygen level–dependent (BOLD) cardiac MRI for myocardial perfusion is limited by inadequate spatial coverage, imaging speed, multiple breath holds, and imaging artifacts, particularly at 3.0 T.

Purpose: To develop and validate a robust, contrast agent–unenhanced, free-breathing three-dimensional (3D) cardiac MRI approach for reliably examining changes in myocardial perfusion between rest and adenosine stress.

Materials and Methods: A heart rate–independent, free-breathing 3D T2 mapping technique at 3.0 T that can be completed within the period of adenosine stress (≤4 minutes) was developed by using computer simulations, ex vivo heart preparations, and dogs. Studies in dogs were performed with and without coronary stenosis and validated with simultaneously acquired nitrogen 13 (^{13}N) ammonia PET perfusion in a clinical PET/MRI system. The MRI approach was also prospectively evaluated in healthy human volunteers (from January 2017 to September 2017). Myocardial BOLD responses (MBRs) between normal and ischemic myocardium were compared with mixed model analysis.

Results: Dogs (n = 10; weight range, 20–25 kg; mongrel dogs) and healthy human volunteers (n = 10; age range, 22–53 years; seven men) were evaluated. In healthy dogs, T2 MRI at adenosine stress was greater than at rest (mean rest vs stress, 38.7 msec ± 2.5 [standard deviation] vs 45.4 msec ± 3.3, respectively; MBR, 1.19 ± 0.08; both, $P < .001$). At the same conditions, mean rest versus stress PET perfusion was 1.1 mL/mg/min ± 0.11 versus 2.3 mL/mg/min ± 0.82, respectively ($P < .001$); myocardial perfusion reserve (MPR) was 2.4 ± 0.82 ($P < .001$). The BOLD response and PET MPR were positively correlated (R = 0.67; $P < .001$). In dogs with coronary stenosis, perfusion anomalies were detected on the basis of MBR (normal vs ischemic, 1.09 ± 0.05 vs 1.00 ± 0.04, respectively; $P < .001$) and MPR (normal vs ischemic, 2.7 ± 0.08 vs 1.7 ± 1.1, respectively; $P < .001$). Human volunteers showed increased myocardial T2 at stress (rest vs stress, 44.5 msec ± 2.6 vs 49.0 msec ± 5.5, respectively; P = .004; MBR, 1.1 msec ± 8.08).

Conclusion: This three-dimensional cardiac blood oxygen level–dependent (BOLD) MRI approach overcame key limitations associated with conventional cardiac BOLD MRI by enabling whole-heart coverage within the standard duration of adenosine infusion, and increased the magnitude and reliability of BOLD contrast, which may be performed without requiring breath holds.

Online supplemental material is available for this article.

Detection of impaired myocardial perfusion reserve (MPR) is valuable in the clinical management of coronary artery disease (1). SPECT and PET imaging methods are the established standards in helping to determine myocardial perfusion; however, these approaches require ionizing radiation and alternate methods are sought. Therefore, first-pass perfusion cardiac MRI, particularly incorporating recent technical advances (motion correction, dark-rim artifact reduction, spatial coverage) in MRI techniques (2–6), provides evidence that myocardial perfusion can be determined without radiotracers. However, first-pass perfusion cardiac MRI requires gadolinium-based contrast agents, which is contraindicated in patients with late-stage chronic kidney disease (7–9). Moreover, there is a growing concern that gadolinium-based contrast agents can lead to chronic deposition of gadolinium within the myelin sheaths with unknown outcomes even in patients without renal insufficiency (10,11).

There is increasing clinical evidence that blood oxygen level–dependent (BOLD) cardiac MRI helps to assess myocardial perfusion without radiation and exogenous contrast agents. BOLD MRI has been shown to provide details on myocardial perfusion on the basis of differential changes in oxygen saturation between rest and vasodilator

Abbreviations

BOLD = blood oxygen level–dependent, HR = heart rate, IQR = interquartile range, LAD = left anterior descending, MBR = myocardial BOLD response, MPR = myocardial perfusion reserve, SR = saturation recovery, 3D = three-dimensional, 2D = two-dimensional

Summary

Three-dimensional blood oxygen level–dependent cardiac MRI at 3.0 T allowed for assessment of whole-heart myocardial perfusion change between rest and stress.

Key Results

- A three-dimensional (3D) blood oxygen level–dependent (BOLD) MRI method was developed to measure myocardial T2 times before and after stress imaging independent of heart rate. The ratio of T2 times (before and after stress) was defined as the myocardial BOLD response.
- In an animal model of myocardial ischemia, the 3D myocardial BOLD MRI response was greater in normal myocardium versus ischemic myocardium (1.08 vs 1.00, respectively; $P < .001$).
- In healthy volunteers, BOLD response of the normal myocardium was 1.09 (ie, 9% greater T2 signal stress vs rest; $P < .001$).

stress (12–16). Despite these advances, BOLD cardiac MRI is generally limited by compromised spatial coverage caused by insufficient imaging speed, loss in BOLD sensitivity (T1 recovery, coil bias, and heart rate [HR] fluctuations between rest and stress examinations), and imaging artifacts (cardiac and respiratory motion and B_0 and B_1 field inhomogeneity) that are especially prominent at 3.0 T, wherein the myocardial BOLD sensitivity is superior to that at 1.5 T (17). These limitations can compromise the diagnostic sensitivity of BOLD cardiac MRI, resulting in inaccurate interpretation of myocardial perfusion between rest and stress.

To address these limitations, we developed and validated a robust, contrast agent–unenhanced, free-breathing three-dimensional (3D) cardiac MRI approach that can reliably help to identify changes in myocardial perfusion between rest and adenosine stress.

Materials and Methods

The canine studies were approved by the institutional animal care and use committee. For human studies, the protocol was approved by the institutional review board. Participants provided written informed consent in compliance with the Health Insurance Portability and Accountability Act. Animal and human studies were performed prospectively between March 2016 and September 2016 and January 2017 and September 2017, respectively.

MRI Pulse Sequence

An electrocardiography-gated, free-breathing, 3D T2 mapping sequence was developed for whole-body MRI (Magnetom Verio; Siemens Healthineers, Erlangen, Germany) and PET/MRI (Biograph mMR; Siemens Healthineers). To reduce imaging time and improve participant comfort, a saturation recovery (SR) preparation was integrated with a constant SR time to null longitudinal magnetization at every heartbeat (18) to eliminate recovery heartbeats, typically performed with standard T2 preparation protocols (19,20). The fixed SR time ensures that longitudinal magnetization is invariant to HR changes, which can enable accurate T2 measurements at changing HR conditions (eg, rest and stress examinations). To speed data acquisition and enable free-breathing protocol, a motion-correction platform with a hybrid Cartesian-radial trajectory (21) was applied to acquire T2 maps with near perfect imaging efficiency. Examination parameters were as follows: repetition time msec/echo time msec, 3.0/1.5; flip angle, 15°; bandwidth, 100 Hz/pixel; and voxel size, $2.0 \times 2.0 \times 6.0$ mm^3. Three incremental T2 preparation times (0, 24, and 55 msec) were used to reconstruct T2 maps by using a custom-written script (Matlab 9.1 R2016b; Mathworks, Natick, Mass). To ensure that the cardiac phase (end diastole) between rest and stress conditions was matched, a variable trigger delay was imposed. SR time of 310 msec was used to accommodate a maximum HR of 125 beats per minute. Adiabatic T2 preparation and spoiled gradient-echo readouts with centric reordering were used to minimize potential confounding effects from inhomogeneous B_1 and B_0 fields and T1 recovery (22).

Pulse sequence diagram and reconstruction flowchart are shown in Figure 1. Raw data acquired during free-breathing conditions were separated into four respiratory bins with the navigator signal to estimate respiratory motion. Data acquired from all T2 preparation times (effective echo times) were combined to generate composite anatomic images and reduce the streaking artifact from undersampling. In the motion correction platform, corresponding affine transform parameters from each respiratory bin were estimated by using iterative registration of the composite images. These motion estimates were applied to data in each bin, and motion-corrected images were reconstructed with different effective echo times. The signal intensities from the images were fit pixel-wise to a monoexponential model to derive motion-corrected T2 values (21). Our sequence was designed to acquire a 3D whole-heart T2 map within 4 minutes.

Numerical Simulations and ex Vivo Studies

To systematically evaluate the effect of HR fluctuations from the standard and proposed T2-based cardiac MRI examinations, numerical simulations and ex vivo studies were performed. Freshly excised canine hearts ($n = 3$) were immersed in saline solution and individually imaged by using a head coil. Ex vivo images were acquired with the following: a commercially available two-dimensional (2D) T2 mapping sequence (20), the proposed 3D method without SR preparation, and a proposed 3D sequence (which includes SR preparation) triggered by simulated heartbeats with HRs of 40−110 beats per minute in increments of 10 beats per minute. Three-dimensional sequences were prescribed with full left ventricular coverage and 2D sequences were prescribed to the matched 3D partitions. HRs were chosen to capture the typically observed R-R changes between rest and adenosine stress (23). To minimize bias, the prescription order of the sequences was randomized. Computer simulations that used Bloch equations (24), with parameters corresponding to the listed sequences, were also performed for validation purposes. Methodologic details of the

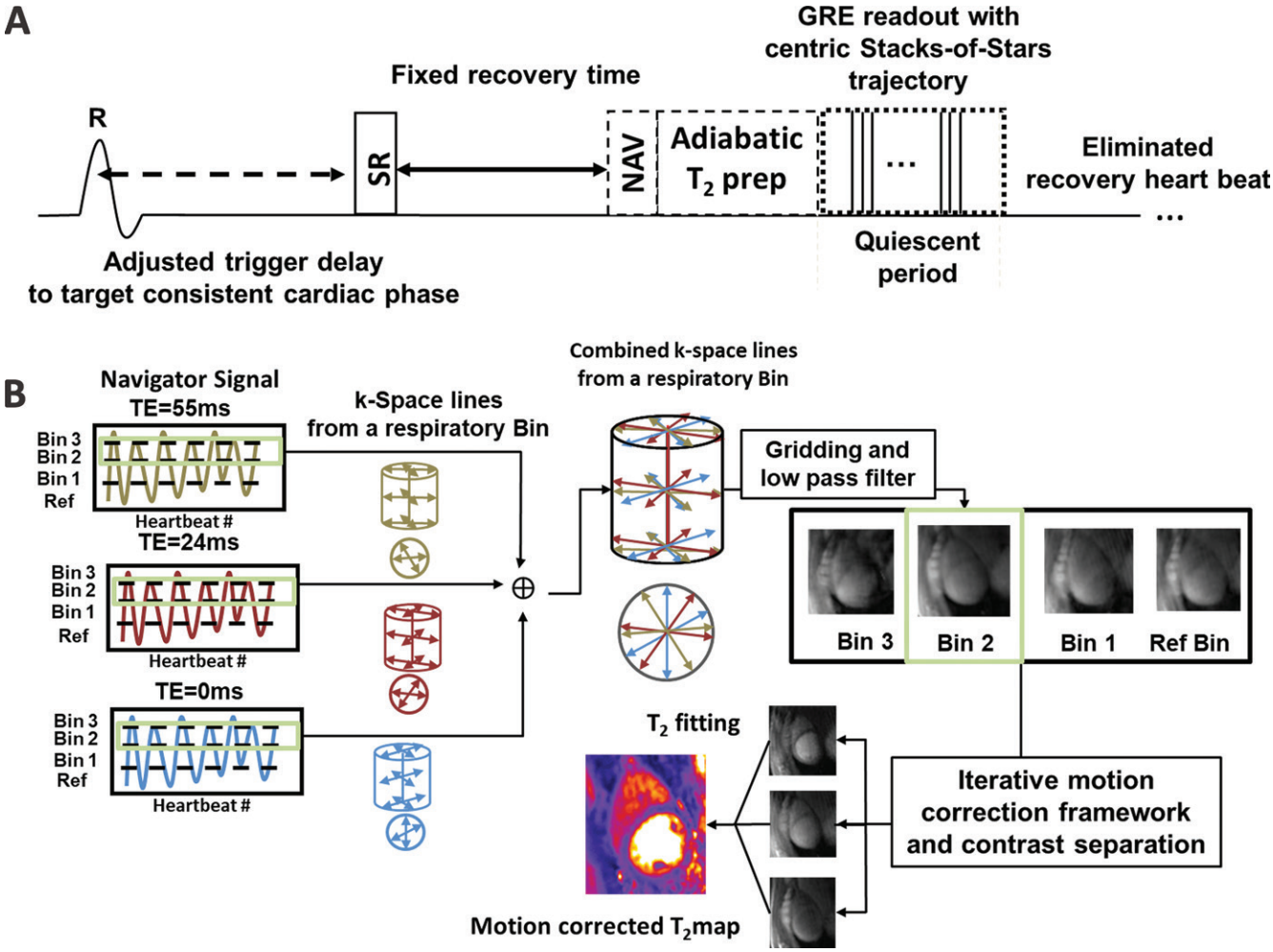

Figure 1: Pulse diagram and reconstruction scheme for the proposed three-dimensional (3D) T2 mapping technique. *A*, The timing diagram. Standard T2 preparation scheme was replaced by a T2 preparation scheme composed of composite adiabatic radiofrequency pulses and spoiled gradient-echo (GRE) readout (in place of the typical balanced steady-state free precession readout) to minimize B_1 and B_0 artifacts at 3.0 T. A centric readout trajectory was applied to ensure optimal T2 weighting. A saturation recovery (SR) pulse preparation was added to eliminate the recovery heart beats on conventional T2 maps and the signal dependence on heart rate between segmented readouts. The respiratory motion was monitored by using a pencil-beam navigator during acquisition. The sequence was designed to permit T2 mapping with three different T2 preparation times for T2 fitting. *B*, Motion correction algorithm used (21). Raw data with different T2-weighted values were first combined and binned on the basis of the navigator signal to generate anatomic images from different respiratory phases. The respiratory motion was estimated from the anatomic images and applied to the raw data to reconstruct motion-corrected T2 maps by using a log-transformed linear least-squares fit as previously described (21). NAV = navigator pulse, TE = echo time, T2 Prep = T2 preparation prepulse.

simulations and ex vivo studies are provided in Appendix E1 (online).

Validation Studies in Dogs

Cardiac MRI studies were performed in dogs (n = 10; body weight, 20–25 kg; mongrel dogs) with and without coronary stenosis, along with simultaneous acquisition of nitrogen 13 (^{13}N)-ammonia PET in the PET/MRI system as described. Two groups of dogs were studied: healthy dogs (group intact, n = 10) and dogs with coronary stenosis (group stenosis, n = 10). For the stenosis studies, animals were implanted with occluders to artificially induce left anterior descending (LAD) stenosis, as previously described (25). Prior to imaging, animals fasted for 18 hours and were sedated, anesthetized with propofol (2.0–5.0 mg/kg, intravenous administration), intubated, moved to the imaging table, and ventilated (Model 2002 Hallowell EMC, Pittsfield, Mass). Electrocardiography, HR, and blood pressure were monitored throughout the studies. Anesthesia was maintained with a continuous infusion of low-dose propofol (0.03–0.1 mg/kg/min, intravenous administration) at imaging to minimize confounding effects of anesthesia on the heart. In group stenosis, imaging was performed after establishing nonflow limiting stenosis at rest (absence of visually evident ST-elevation at rest). Moreover, cine cardiac MRI was performed to ensure that after the release of the LAD stenosis, wall motion abnormalities or edema (26) were absent. All studies were terminated with delayed contrast enhancement cardiac MRI to rule out myocardial infarction. Imaging parameters are provided in Appendix E1 (online).

^{13}N-ammonia PET and BOLD cardiac MRI protocol.—^{13}N-ammonia PET and BOLD cardiac MRI were performed simultaneously by using the same imaging system (PET and cardiac MRI data acquisition details are in Appendix E1 [online]).

To investigate the influence of HR on BOLD sensitivity, 2D T2 mapping was performed on a single midventricular section in the intact animals and was randomized with respect to the acquisition order (ie, before or after 3D acquisitions). In group intact, images were acquired during adenosine infusion (140 μg/kg/min, intravenous administration]) and at rest to determine the MPR and myocardial BOLD response (MBR). Specifically, by using adenosine, image acquisitions were prescribed after 2 minutes of the 6 minutes of adenosine infusion. In group stenosis, images were acquired at rest and with adenosine after inducing LAD coronary stenosis. Other aspects of the imaging protocol implemented in group stenosis were similar to those implemented in group intact. A schematic representation of the sequential execution of the study protocols is provided in Appendix E1 (online). Once the imaging was completed, animals were humanely killed.

Whole-heart BOLD Cardiac MRI in Healthy Volunteers

Healthy volunteers (n = 10; age range, 22–53 years; seven men) were examined by using the whole-body 3.0-T MRI system as indicated. Study participants were placed in the supine position, and after scouting and whole-heart shimming, the proposed sequence was performed at rest and 2 minutes after the start of adenosine infusion (140 μg/kg/min, intravenous administration; total infusion time, 6 minutes). Imaging parameters, including the SR and T2 preparation schemes, were the same as those used for canine studies.

Image Analysis

MRI images were analyzed with an opensource software (ImageJ version 1.46; National Institutes of Health, Bethesda, Md) and in-house Matlab scripts (Matlab; Mathworks). PET images were analyzed with a commercially available software (QPET v.2017; CSMC, Los Angeles, Calif). Images were analyzed by two authors (H.J.Y. and D.D., both with > 10 years of experience in cardiac imaging research). Consensus from both readers was reached for all image contours. Readers were blinded from the acquisition protocols and physiologic conditions of the participants.

Ex vivo analysis.—T2 measured within the regions of interest on the midventricular myocardial images acquired at the different sequences at variable HRs were used evaluate the dependence of T2 on HR.

Ammonia PET.—All ^{13}N-ammonia PET images were processed by an experienced technologist (J.B., with > 10 years of experience in cardiac PET imaging) as previously described (27). Myocardial perfusion (in milliliter per minute per gram) and MPR were quantified automatically from the PET data by using commercially available software (QPET; Cedars-Sinai Medical Center, Los Angeles, Calif) (27). In group stenosis, myocardial segments with perfusion defects were identified on the basis of stress-rest change analysis in QPET (27,28). The segments identified with perfusion deficit were labeled as ischemic and those without perfusion defects were labeled as normal segments.

BOLD cardiac MRI.—Epicardial and endocardial contours were traced on T2 maps to delineate the myocardium and were subsequently segmented according to the American Heart Association 16-segment model by using ImageJ (National Institutes of Health). Mean myocardial T2 values at rest and stress were measured for each segment with custom scripts (Matlab; Mathworks). MBRs were defined as T2 at stress normalized by the T2 at rest (MBR = $T2^{Stress}/T2^{Rest}$) for each segment. This was determined in both group of animals (intact and stenosis) and compared with segmental MPR from ^{13}N-ammonia PET. In the intact group, MBRs were computed from the T2 maps of midventricular sections acquired by using the proposed approach that were matched to the 2D T2 maps. For stenosis studies, MBR of the ischemic segments (identified on the basis of ^{13}N-ammonia PET analysis [27,28]) were compared against the MPR of the normal segments. A similar analysis was performed in human volunteers to determine MBR. In addition, to investigate the influence of HR fluctuations between rest and stress (change in HR = $HR^{Stress} - HR^{Rest}$) at BOLD response, [loss of apparent MBR = 100% · ($MBR_{Prop} - MBR_{Conv}$)], where MBR_{prop} is the proposed approach and MBR_{conv} is proposed approach that was matched to the 2D T2 maps, was computed and regressed against change in HR. Image quality between the proposed and the conventional 2D T2 maps obtained from dogs and humans were not different (Appendix E1 [online]).

Statistical Analysis

Statistical analysis was performed by using commercially available software (SPSS V21.0; IBM, Armonk, NY), and P values less than .05 were considered to indicate statistical significance. For ex vivo studies, the 2D T2 maps acquired at HR of 60 beats per minute were labeled as baseline. T2 measurements at various fixed HRs were compared with baseline values by using two-way repeated measures analysis of variance. The normality of T2 values was tested by using the Shapiro-Wilk test, and the normality could not be rejected. For the intact animal studies, paired t tests were used to compare myocardial PET perfusion and T2 values between rest and stress by using midventricular sections (segmented according to AHA model) so as to not be confounded by the contamination by the valve plane (at PET) in the basal sections and to minimize the effects of resolution differences between PET and MRI in the apical sections. A repeated measure correlation analysis (29) was performed to examine the data trends between MBR and MPR by using the R package (rmcorr v0.3.0; R Project for Statistical Computing, *https://CRAN.R-project.org*). Linear regression between loss of apparent BOLD contrast and change in HR was performed to investigate the influence of HR changes on BOLD response. For the stenosis studies, MPR from the ischemic and normal segments in all animals was compared by using a mixed-model analysis. The same test was used to examine the difference in the simultaneously acquired MBR. In human studies, segmental T2 values between rest and stress were compared by using a paired t test, and a t test was used to test whether MBR was greater than one. In cases with subject-based mea-

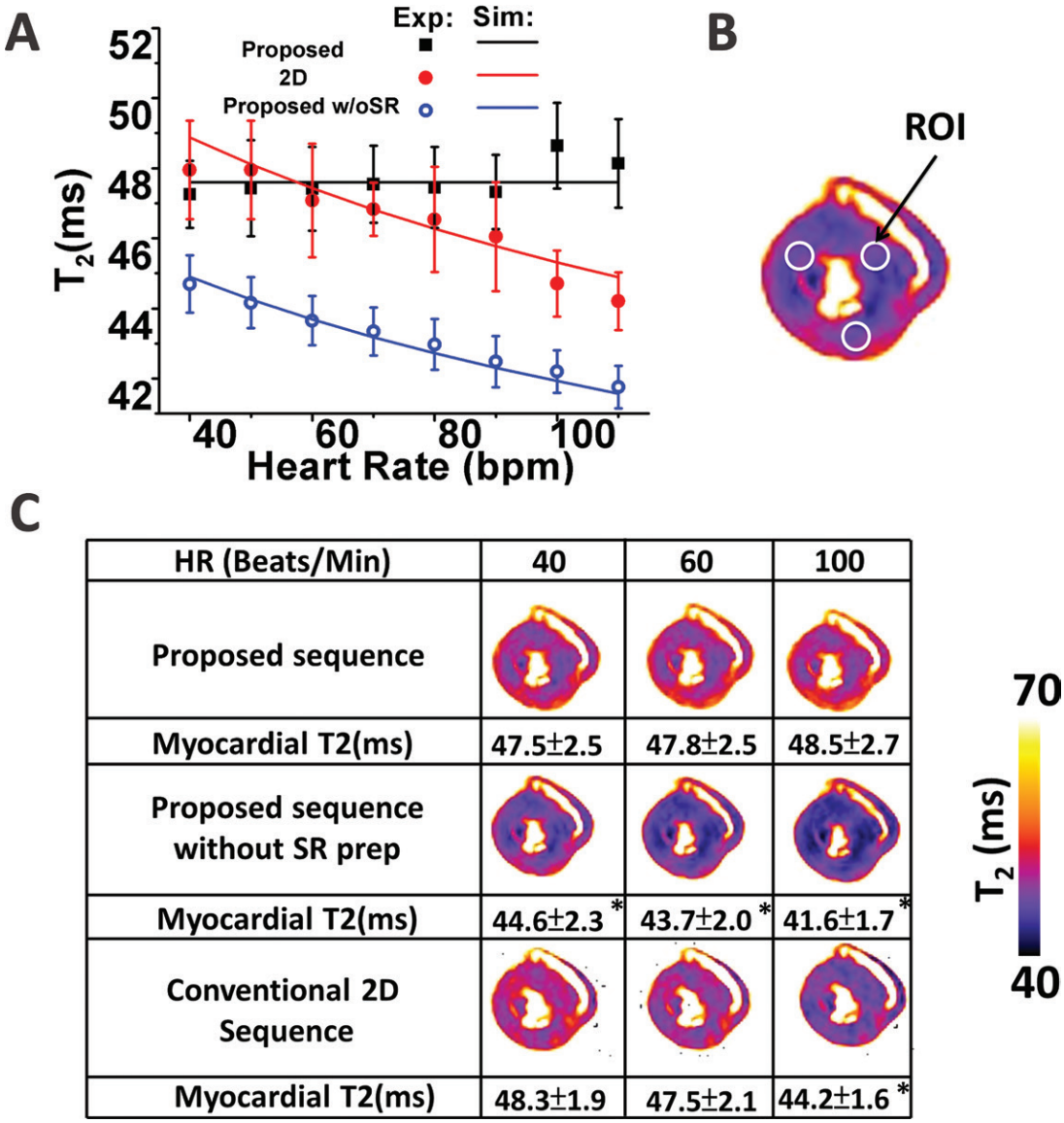

Figure 2: T2 dependence on heart rate as determined from computer simulations and ex vivo studies ($n = 3$). *A*, The theoretically expected dependence of T2 on heart rate for the two-dimensional (2D) and three-dimensional (3D) T2 mapping without saturation recovery (SR; proposed without [w/o] SR) and with SR preparation (proposed) are shown as solid lines. Experimentally measured T2 values from ex vivo hearts at the different artificially modulated heart rates are also shown in *A*. *B*, Representative regions of interest (ROI) used for the analysis are identified for reference. *C*, A set of representative midventricular T2 maps acquired by using the different T2 mapping approaches is shown. Underestimated T2 values under elevated heart rate (100 beats per minute [bpm]) are observed on 2D T2 maps and 3D T2 maps without SR preparation (both $P < .05$). The effect is eliminated with the proposed 3D T2 mapping approach ($P = 1$). All T2 values were compared with the T2 value measured with the baseline values. All images showed consistent image quality and similar T2 distribution. * $P < .05$. Exp = experimental results, Sim = simulated results.

surements, numbers were reported with medians and interquartile ranges (IQRs) unless stated otherwise.

Results

Computer Simulations and ex Vivo Study

Figure 2 shows the results from computer simulations and the ex vivo studies. Simulated and experimental mean myocardial T2 values measured with artificially modulated HRs were compared (Fig 2, *A*). Simulations showed a negative correlation between T2 values and HRs ($P < .001$), which was not evident with our proposed sequence ($P > .99$). Experimental T2 values measured from regions of interest placed within the midventricular sections (Fig 2, *B*) confirmed the predictions of computer simulations. A representative set of midventricular short-axis T2 maps acquired with the different T2 mapping strategies at various HRs is shown in Figure 2, *C*. Myocardial T2 measured with the conventional T2 mapping sequence at HR of 60 beats per minute was labeled as the baseline myocardial T2. On T2 maps acquired with 2D imaging and our proposed approach without SR preparation, T2 underestimation was observed at typical stress HRs compared with baseline

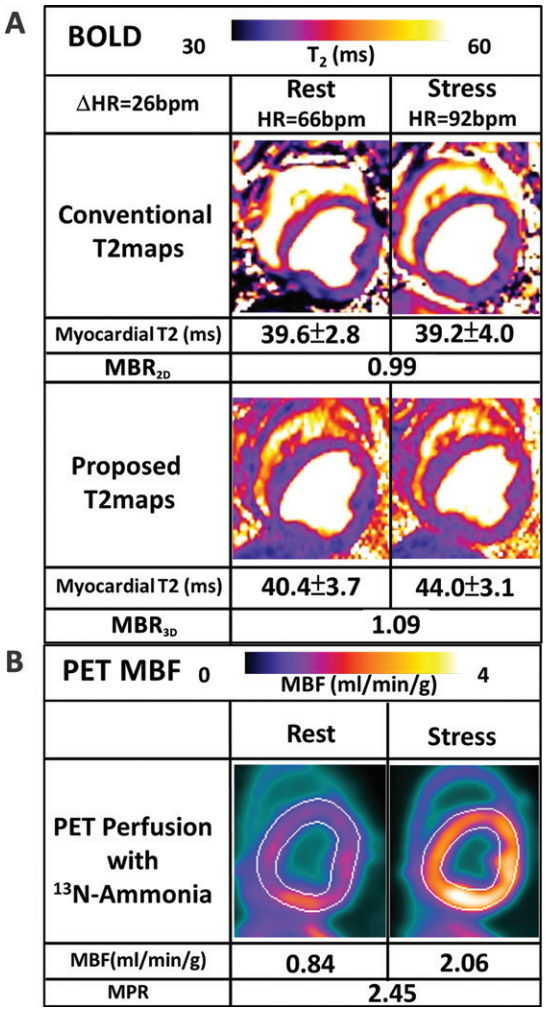

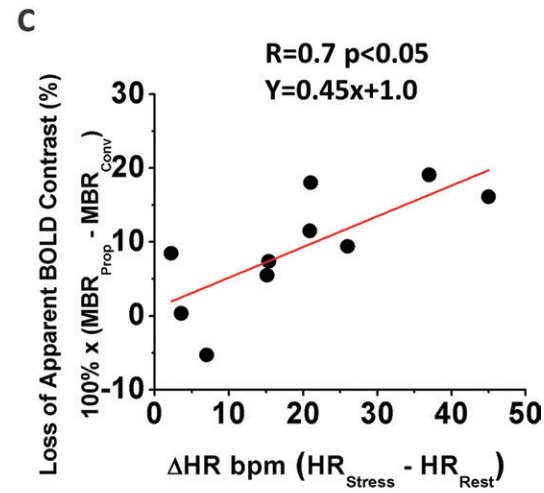

Figure 3: Dependence of myocardial blood oxygen level–dependent (BOLD) response (MBR) sensitivity on heart rate differences between rest and vasodilator stress (n = 10). *A*, Representative rest and stress T2 maps of a midventricular section obtained at two-dimensional (2D) imaging and proposed three-dimensional (3D) T2 mapping methods are shown. Myocardial T2 under stress with the proposed T2 mapping approach is much higher than T2 at rest but T2 under stress is reduced in the 2D images compared with rest. *B*, Myocardial blood flow (MBF), derived from PET, in the same animal; MBF is higher under stress with an myocardial perfusion reserve (MPR) larger than 2 (P = .001). *C*, Experimentally observed relationship between loss of apparent MBR on 2D images and heart rate (HR) increases with vasodilator stress. A strong positive correlation was observed between loss of apparent MBR and change in HR (ΔHR). Data in *A* and *B* are means ± standard deviation. bpm = beats per minute.

HR (median 2D, 47.2 msec [IQR, 46.1–48.9 msec; HR, 60 beats per minute] vs 47.4 msec [IQR, 46.4–49.9 msec; HR, 100 beats per minute], respectively; mean 2D, 47.6 msec ± 2.1 [standard deviation] vs 48.5 ± 2.7, respectively; median 3D without SR, 43.4 msec [IQR, 43.1–44.8; HR, 60 beats per minute] vs 41.6 msec [IQR, 40.4–42.3 msec; HR, 100 beats per minute], respectively; mean 3D without SR, 43.7 msec ± 1.0 vs 41.6 msec ± 1.8; both $P < .001$). However, images acquired with SR preparation showed no correlation to HR ($P > .99$). T2 values acquired with the proposed approach did not differ from T2 estimates obtained by using 2D T2 at baseline HR of 60 beats per minute (all $P > .8$).

Animal Studies

The dependence of loss of apparent MBR on change in HR is shown on Figure 3. Figure 3, *A*, shows a representative set of section-matched rest and stress midventricular images obtained with the proposed and 2D sequences. In this example, an HR increase of 26 beats per minute in response to adenosine stress led to a 9% increase in MBR with the proposed approach, whereas a 1% decrease in MBR occurred with the 2D T2 mapping approach. Results from measurements at PET of the myocardial blood flow in the same animal are shown in Figure 3, *B*. The corresponding global MPR in this animal was 2.45, which demonstrates the presence of marked vasodilation that is depicted by the proposed method but not captured by 2D T2 mapping approach. Figure 3, *C*, shows positive correlation between the loss of apparent MBR and change in HR (R = 0.71; $P < .05$), which indicates that the larger the HR change (from rest) in response vasodilator stress, the greater the loss of apparent MBR on T2 maps that are uncorrected for HRs.

MBR and MPR in dogs without coronary stenosis after adenosine administration were consistently higher than at rest. Figure 4 shows representative sets of short-axis T2 maps depicting BOLD response and ^{13}N-ammonia PET perfusion (Fig 4, *A*) acquired at rest and adenosine stress. Corresponding bull's eye plots derived from segmental intensities are shown in Figure 4, *B*, *C*, for BOLD cardiac MRI and ^{13}N-ammonia PET. Mean MBRs from segmental intensities for BOLD cardiac MRI and ^{13}N-ammonia PET MPR were as follows: 1.19 ± 0.08 (median, 1.18; IQR, 1,14–1.21) and 2.5 ± 0.7 (median, 2.7; IQR, 2.2–2.8), respectively. Absolute mean myocardial T2 and ^{13}N-ammonia PET perfusion values at rest and adenosine stress for all intact animals are shown in Figure 5, *A*, *B*, respectively. BOLD response and MPR from each segment are compared in Figure 5, *C*. ^{13}N-ammonia PET perfusion values were higher at adenosine stress than at rest (mean rest vs stress, 1.1 mL/mg/min ± 0.11 [median, 1.1; IQR, 1.06–1.14 mL/mg/min] vs 2.3 mL/mg/min ± 0.82

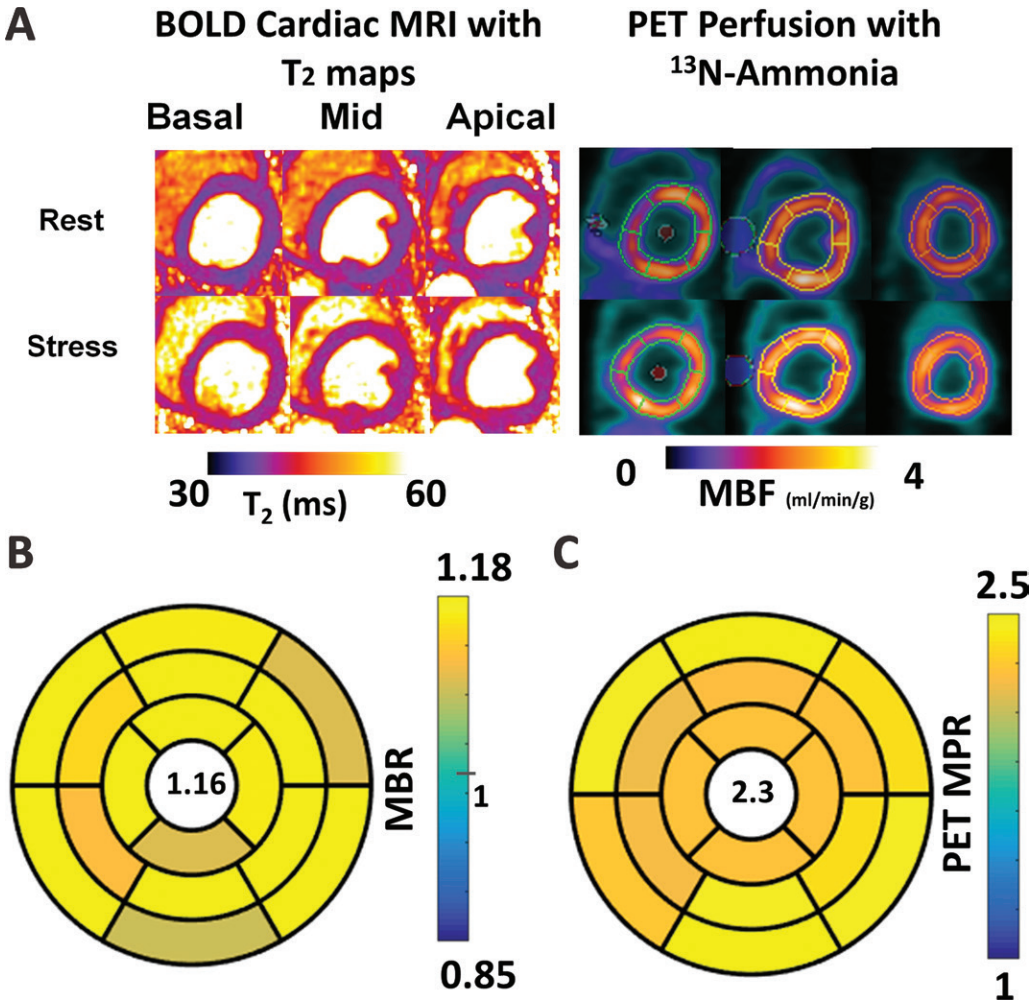

Figure 4: Three-dimensional (3D) T2 maps and nitrogen 13 (^{13}N)-ammonia PET at rest and under adenosine stress in dogs without coronary stenosis. *A*, Representative basal, middle, and apical short-axis images from blood oxygen level–dependent (BOLD) cardiac MRI with the proposed 3D T2 mapping approach and PET perfusion images in a dog with ^{13}N-ammonia are shown. From images acquired by using both modalities, signal elevation can be observed on the stress images compared with the corresponding rest images ($P < .001$). Corresponding bull's eye plots in the same subject are shown (myocardial BOLD response [MBR], *B*, and PET MBR, *C*). Mean BOLD response of 16% and PET myocardial perfusion reserve (MPR) of 2.3 were evident in the whole heart. MBF = myocardial blood flow.

[median, 2.1; IQR, 1.74–2.33 mL/mg/min], respectively; $P <$ .001; Fig 5, *B*). The corresponding mean MPR was 2.4 mL/mg/min ± 0.82 (median, 2.2; IQR,1.74–2.63 mL/mg/min). Myocardial T2 was higher at adenosine stress (mean rest vs stress, 38.7 msec ± 2.5 [median, 39.4 msec; IQR, 36.6–41.4 msec] vs 45.4 msec ± 3.3 [median, 44.1 msec; IQR, 42.6–48.3 msec], respectively; $P < .001$; Fig 5, *A*) with a mean MBR of 18% ± 10 (median, 18%; IQR, 11%–21%). The segmental MBR and ^{13}N-ammonia PET MPR was positively correlated ($R = 0.67$; $P < .001$).

In group stenosis, a representative set of short-axis T2 maps depicting BOLD response and the corresponding rest and stress ^{13}N-ammonia PET perfusion in a dog with LAD stenosis are shown in Figure 6, *A*, *D*, respectively. T2 maps acquired with adenosine showed a reduction in T2 in the LAD (ischemic) territories of midventricular and apical sections (ischemic vs normal, 38.5 msec ± 0.7 [median, 39.3 msec; IQR, 32.0–42.8 msec] vs 42.0 msec ± 0.66 [median, 42.5 msec; IQR, 37.5–47.0 msec]; $P = .01$). Myocardial blood flow reduction in the same territories in the ^{13}N-ammonia PET was observed (normal vs ischemic at rest: 1.16 mL/mg/min ± 0.53 [median, 1.04 mL/mg/min; IQR, 0.81–1.60 mL/mg/min] vs 1.05 mL/mg/min ± 0.56 [median, 0.93 mL/mg/min; IQR, 0.66–1.39 mL/mg/min]; $P = .6$; normal vs ischemic at stress: 2.59 mL/mg/min ± 1.03 [median, 1.99 mL/mg/min; IQR, 1.93–3.61 mL/mg/min] vs 1.43 mL/mg/min ± 0.72 [median, 1.15 mL/mg/min; IQR, 0.99–1.71 mL/mg/min]; $P = .002$). Polar plots of MBR and MPR are shown in Figure 6, *B*, *E*, respectively, which show reduced MBR and MPR in a dog with LAD coronary stenosis. Box plots of MBR and MPR in the normal and ischemic segments are shown in Figure 6, *C*, *F*. Mean MBR and MPR of the ischemic territories were lower than the normal territories (normal vs ischemic MBR: 1.09 ± 0.05 [median, 1.08; IQR, 1.05–1.12] vs 1.00 ± 0.04 [median, 1.00; IQR, 0.98–1.02]; $P < .001$; and normal vs ischemic MPR: 2.7 ± 0.08 [median, 2.7; IQR, 1.9–2.6] vs 1.7 ± 1.1 [median, 1.5; IQR, 1.4–2.3]; $P < .001$).

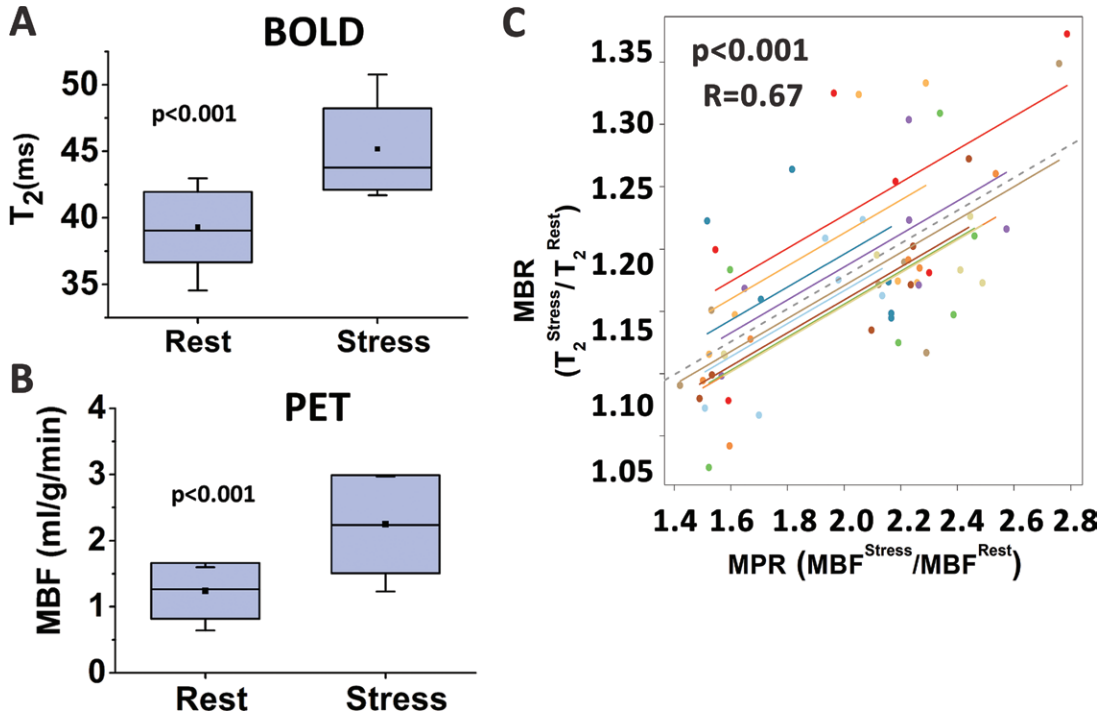

Figure 5: Mean blood oxygen level–dependent (BOLD) response and nitrogen 13 (^{13}N)-ammonia PET perfusion in dogs without coronary stenosis (n = 10). *A*, Box and whisker plot with higher mean myocardial T2 values at adenosine stress compared with rest (rest vs stress, 39.4 msec [interquartile range, 36.6–41.4 msec] vs 44.1 msec [interquartile range, 42.6–48.3 msec], respectively; $P < .001$). *B*, A similar trend is observed with ^{13}N-ammonia PET perfusion measurements (rest vs stress, 1.1 mL/mg/min [interquartile range, 1.06–1.14 mL/mg/min] vs 2.1 mL/mg/min [interquartile range, 1.74–2.33 mL/mg/min], respectively; $P < .001$). *C*, Scatterplot comparing BOLD response (on the y-axis) compared with ^{13}N-ammonia PET myocardial perfusion reserve (MPR). Each color represents segmental measurements (points) and regressed lines (lines) from one dog. Paired t test showed significant difference in myocardial BOLD responses (MBRs) and MPRs between rest and stress (both $P < .001$). A repeated measure correlation analysis to examine the data trends between MBR and MPR at the segmental level. The result showed a positive correlation between MBR and MPR ($R = 0.67$; $P < .001$). MBF = myocardial blood flow.

Human Studies

Each of the stress and rest examinations were completed within 4 minutes. Rest myocardial T2 from our proposed method is consistent with the T2 values measured with 2D T2 maps (2D vs 3D, 42.1 msec ± 4.5 [median, 42.7 msec; IQR, 38.7–44.7 msec] vs 44.5 msec ± 2.6 [median, 44.4 msec; IQR, 42.1–46.5 msec], respectively; P = .9). Increases in myocardial T2 were observed at stress compared with rest (stress vs rest, 49.0 msec ± 5.5 [median, 47.9 msec; IQR, 45.2–52.3 msec] vs 44.5 msec ± 2.6 [median, 44.4 msec; IQR, 42.1–46.5 msec], respectively; P = .004). Mean MBR in the study participants was 1.1 ± 0.08 (median, 1.09; IQR, 1.04–1.16). Representative short-axis images in a healthy volunteer with a corresponding polar map representation of MBR are in Figure 7, *A*, *B*. All three images showed visually discernable increases in T2 at stress compared with rest. Box plots with paired BOLD response are shown for each participant in Figure 7, *C*, with paired t test showing that there was a statistically significant increase across in T2 following adenosine stress (P = .004).

Discussion

Blood oxygen level–dependent (BOLD) cardiac MRI is a contrast-unenhanced method that may be useful for depicting the presence of hypoperfused myocardial territories. However, the most commonly used T2-based BOLD cardiac MRI methods have well-known limitations including inadequate spatial coverage during vasodilator stress, heart rate (HR) variations between rest and stress acquisitions, and limited validation. In our study, we developed a T2-based BOLD cardiac MRI approach at 3.0 T to overcome these key imitations. Our proposed approach permitted full left ventricular coverage within the duration of adenosine stress at free-breathing conditions with T2 values that were not different from breath-held two-dimensional (2D) T2 maps at rest ($P > .8$, in ex vivo hearts, dogs, and humans volunteers), preserves BOLD sensitivity independent of HR variations between rest and stress (P = 1), and results in BOLD response that is consistent with blood flow response as observed in simultaneously acquired nitrogen 13 (^{13}N)-ammonia PET acquired at identical physiologic conditions of stress and rest ($R = 0.67$; $P < .001$).

Our 3D BOLD cardiac MRI method was compared with an established 2D T2 mapping approach (20) and the 3D T2 mapping without the SR preparation. By using an SR preparation, we ensured a common starting point for longitudinal evolution of magnetization during each of the segmented readouts, thereby removing the variability associated with longitudinal signal recovery at rest and stress. This dependence of HR on T2 has an important implication for BOLD cardiac MRI: it can underestimate the expected BOLD response in proportion to change in HR.

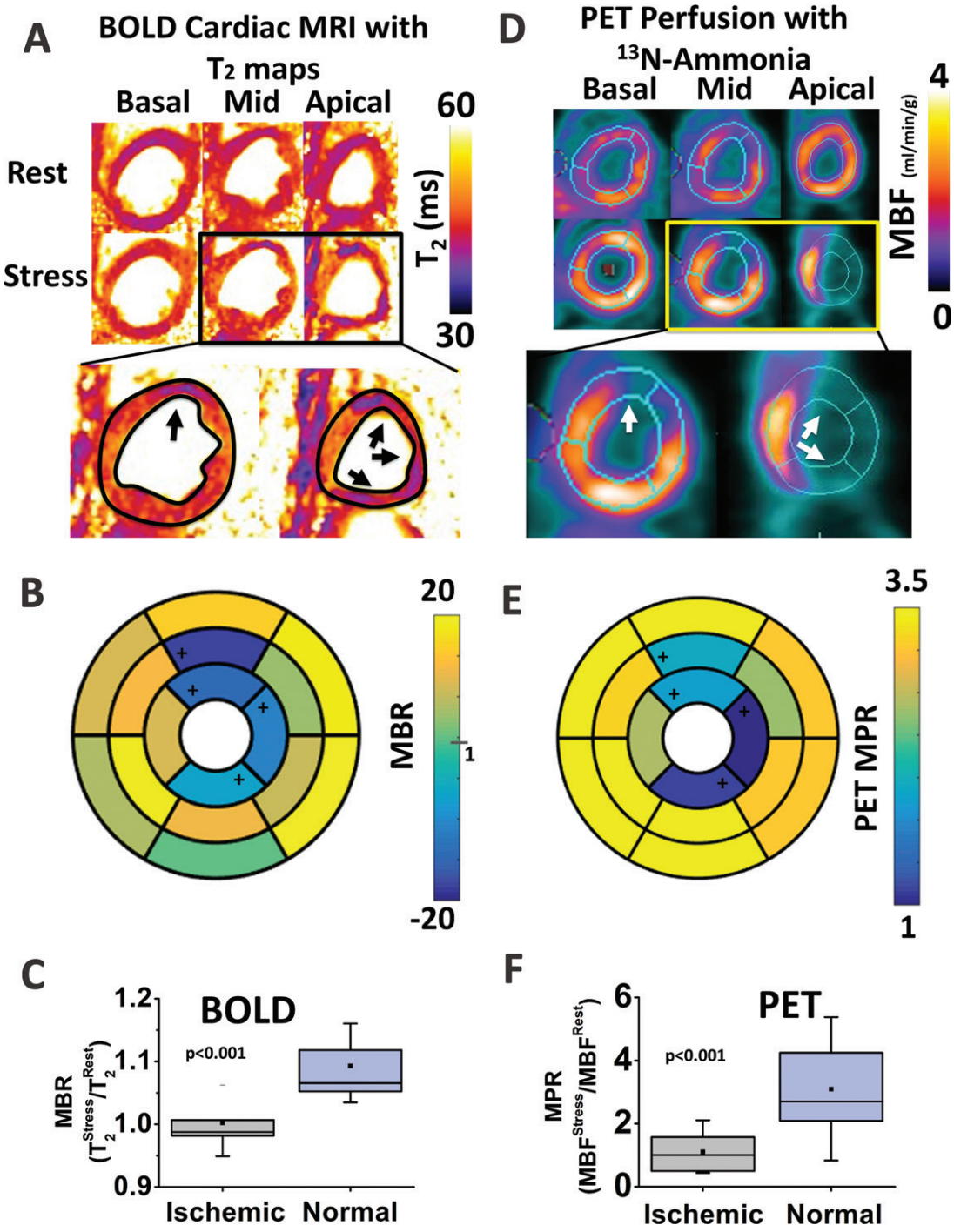

Figure 6: Three-dimensional T2 maps and nitrogen 13 (^{13}N)-ammonia PET at rest and under adenosine stress in a dog with left anterior descending (LAD) coronary stenosis. *A*, Representative basal, middle, and apical short-axis T2 maps at rest and under stress in a dog with LAD coronary stenosis. *D*, The corresponding quantitative myocardial blood flow (MBF) maps determined from ^{13}N-ammonia PET. There is close correspondence in the MBF distribution and T2 maps, particularly at adenosine stress. Specifically, the normal territories on PET images showed increased T2 values on T2 maps acquired with adenosine. Conversely, the ischemic territories on PET images (anterior wall corresponding to LAD territory; white arrows on *D*) showed markedly diminished increase in T2 (black arrows on *A*) compared with normal segments. Corresponding polar maps for, *B*, blood oxygen level dependent (BOLD) and, *E*, PET are shown. Ischemic segments identified with change analysis from QPET are labeled on the polar maps (+ on *B* and *E*). Both, *C*, BOLD response and, F, PET myocardial perfusion reserve (MPR) showed lower values in the ischemic territories compared with the normal segments. Mixed-model analysis showed lower myocardial BOLD response (MBR; $P < .001$) and MPR ($P < .001$) on ischemic territories.

Effectively, this underestimation at T2 counters the vasodilator-mediated increase in T2, leading to a diminished and unreliable BOLD response, which may partly account for the large scatter that is typically observed between T2-based BOLD cardiac MRI and perfusion studies in the literature. These variations might also lead to incorrect estimation of

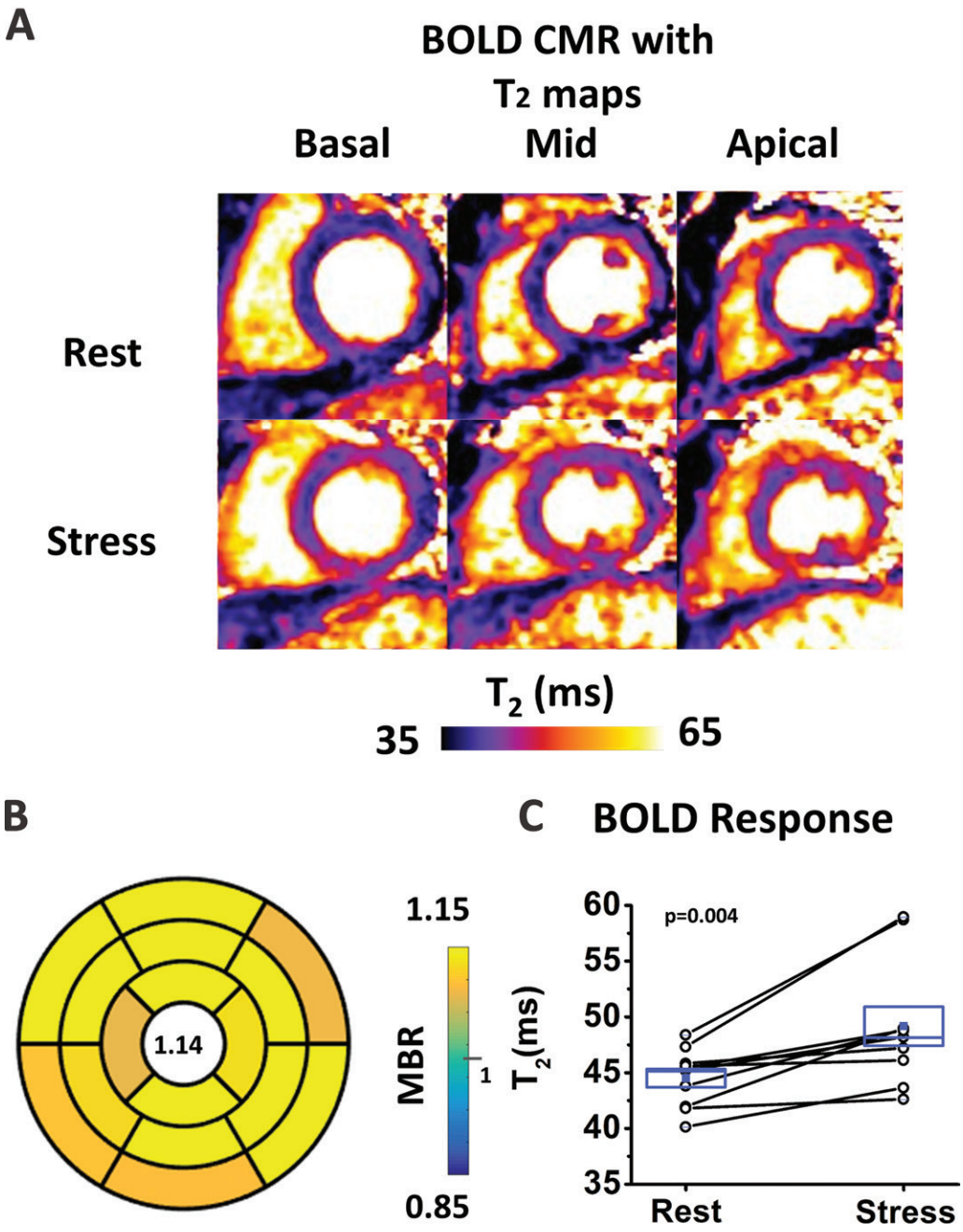

Figure 7: Heart rate–independent three-dimensional T2 mapping at rest and at adenosine stress in healthy human participants (*n* = 10). *A*, Representative short-axis T2 maps at rest and stress in a single participant. An increased myocardial T2 corresponding to hyperemia can be observed across all sections. *B*, Polar map of myocardial blood oxygen level–dependent (BOLD) response (MBR) for the T2 maps corresponding to *A*; the polar maps show a relatively homogenous MBR greater than 1 (across all segments). *C*, Plots of myocardial T2 values across human subjects at rest and stress. Paired *t* test showed higher myocardial T2 under stress compare with rest (stress vs rest, 47.9 msec [interquartile range, 7.1 msec] vs 44.4 msec [interquartile range, 4.4 msec], respectively; *P* = .004.). CMR = cardiac MRI.

myocardial oxygen extraction fraction (30) and potentially complicate interpretations.

Previous studies recognized these limitations and attempted to correct for signal measurements by using fixed model parameters that are often variable between individuals and imaging conditions (12,14,15), which can lead to further misinterpretations. Cardiac phase-resolved BOLD MRI, which is performed in cine mode, is another way to reduce the HR dependency because the examinations are performed at steady state (31,32). However, some of the limitations of this approach are that off-resonance artifacts (particularly at 3.0 T) require breath holding during examination and there is insufficient spatial coverage at vasodilator stress. Our method enables a fast 3D free-breathing examination while eliminating the HR dependency with an SR preparation.

We were able to consistently acquire whole-heart T2 maps within 4 minutes during adenosine infusion without compromising the spatial resolution that is standard in 2D T2 maps. Our data showed that the T2 values in the healthy myocardium measured at rest by using our approach were in good agreement with previous reports in the literature (33,34). Simultaneously acquired T2 and ^{13}N-ammonia PET data, which were used to estimate MBR and MPR, respectively, were positively correlated. In the presence of LAD stenosis, consistent with the findings from ^{13}N-ammonia PET MPR, we observed marked reduction in MBR in the ischemic territories compared with normal territories. Collectively, these findings support that the measures of MBR on the basis of our approach and MPR provide similar information regarding myocardial perfusion and can be used to improve the identification of myocardial territories subtended by coronary arteries with nonflow limiting (at rest) stenosis. Further, we demonstrated the feasibility of our approach for consistently generating artifact-minimized whole-heart T2 maps from free-breathing acquisitions at rest and standard duration of peak adenosine stress (ie, within 4 minutes) in healthy human volunteers. Although the MBR estimates from human participants were not validated against PET MPR, the observed mean MBR of 10% in the human volunteers was comparable to our findings in healthy dogs.

One notable difference between MPR with PET and MBR on the basis of cardiac BOLD MRI is the dynamic range of the responses. Because our goal was to reliably depict BOLD responses, the options to improve detectability are to increase the BOLD response and reduce contributions from confounders. On the basis of theoretical conjectures, it appears the BOLD sensitivity is tied to the field strength (17). Whereas moving to higher field strengths can increase the MBR, this is not a viable option for multiple reasons, primarily because of the lack of high-field-strength imaging systems that can be used for cardiac imaging. Thus, in our study we focused our efforts on improving the reliability of MBR. Notably, we showed that the confounding effects of HR changes between rest and stress are statistically significant and can markedly reduce image contrast. This likely explains the improvement in the relation between cardiac BOLD response and perfusion. Whereas our technical improvements have increased the reliability of the approach, additional strategies of this nature can accentuate the capability of MBR to depict even moderate changes in myocardial perfusion.

Our study had some limitations. It was performed in animal models and healthy human volunteers, which offered well-controlled environments compared with the clinical setting. Although we were able to consistently acquire whole-heart T2 maps within an acceptable window of adenosine stress and eliminate HR dependency, rapid HR and respiratory pattern changes during the examination can cause additional artifacts. Although these challenges may be addressed by using strategies similar to arrhythmia and navigator rejection approaches previously used in other settings (35), we did not use these strategies in our study. Further PET and BOLD cardiac MRI data showed good but not perfect correlation ($R = 0.67$). Potentially there are other technical and/or physiologic factors contributing to this imperfect correlation. From the technical standpoint, further decreases in imaging and physiologic noise, improvements in B_0 and B_1 field inhomogeneities, and improved myocardial segmentation may help to increase this correlation. There may also be physiologic differences between myocardial perfusion determined on the basis of PET and myocardial perfusion determined from BOLD MRI. Thus, the exact source of this imperfect correlation remains to be investigated. Despite this, the technical improvements proposed in our study showed that the correction between MPR and MBR (previously reported to be $R = 0.26$ [14]) can be significantly improved (to $R = 0.67$, as reported here).

In conclusion, our proposed three-dimensional blood oxygen level–dependent cardiac MRI approach offers the capability to acquire artifact-minimized, free-breathing images of the whole left ventricle at peak adenosine stress with no loss in sensitivity from heart-rate changes between rest and stress. Patient studies are necessary for clinical translation.

Acknowledgment: We thank Hao Ho, PhD, for the statistical elements of this study.

Author contributions: Guarantors of integrity of entire study, H.J.Y., R.D.; study concepts/study design or data acquisition or data analysis/interpretation, all authors; manuscript drafting or manuscript revision for important intellectual content, all authors; approval of final version of submitted manuscript, all authors; agrees to ensure any questions related to the work are appropriately resolved, all authors; literature research, H.J.Y., X.B., I.C., R.T., P.S., F.S.P.; clinical studies, H.J.Y., D.D., R.T.; experimental studies, H.J.Y., D.D., J.S., J.B., M.K., B.S., I.C., R.T., F.S.P., R.D.; statistical analysis, H.J.Y.; and manuscript editing, H.J.Y., D.D., M.K., X.B., B.S., I.C., R.T., P.S., F.S.P., R.D.

Disclosures of Conflicts of Interest: **H.J.Y.** disclosed no relevant relationships. **D.D.** disclosed no relevant relationships. **J.S.** disclosed no relevant relationships. **J.B.** disclosed no relevant relationships. **H.B.** disclosed no relevant relationships. **M.K.** disclosed no relevant relationships. **X.B.** Activities related to the present article: disclosed no relevant relationships. Activities not related to the present article: disclosed employment from Siemens Medical Solutions. Other relationships: disclosed no relevant relationships. **B.S.** disclosed no relevant relationships. **I.C.** disclosed no relevant relationships. **R.T.** disclosed no relevant relationships. **P.S.** Activities related to the present article: disclosed no relevant relationships. Activities not related to the present article: disclosed money to author's institution for grants/grants pending from Siemens and National Institutes of Health; disclosed royalties from Cedars-Sinai. Other relationships: disclosed no relevant relationships. **F.S.P.** disclosed no relevant relationships. **R.D.** disclosed no relevant relationships.

References

1. Hachamovitch R. Impact of ischemia and scar on therapeutic benefit of myocardial revascularization. Herz 2013;38(4):344–349.
2. Sharif B, Dharmakumar R, LaBounty T, et al. Towards elimination of the dark-rim artifact in first-pass myocardial perfusion MRI: removing Gibbs ringing effects using optimized radial imaging. Magn Reson Med 2014;72(1):124–136.
3. Zhou R, Yang Y, Mathew RC, et al. Free-breathing cine imaging with motion-corrected reconstruction at 3T using SPiral Acquisition with Respiratory correction and Cardiac Self-gating (SPARCS). Magn Reson Med 2019;82(2):706–720.
4. Wang H, Adluru G, Chen L, Kholmovski EG, Bangerter NK, DiBella EV. Radial simultaneous multi-slice CAIPI for ungated myocardial perfusion. Magn Reson Imaging 2016;34(9):1329–1336.
5. Atkinson DJ, Burstein D, Edelman RR. First-pass cardiac perfusion: evaluation with ultrafast MR imaging. Radiology 1990;174(3 Pt 1):757–762.
6. Otazo R, Kim D, Axel L, Sodickson DK. Combination of compressed sensing and parallel imaging for highly accelerated first-pass cardiac perfusion MRI. Magn Reson Med 2010;64(3):767–776.
7. Hakeem A, Bhatti S, Chang SM. Screening and risk stratification of coronary artery disease in end-stage renal disease. JACC Cardiovasc Imaging 2014;7(7):715–728.
8. Di Angelantonio E, Chowdhury R, Sarwar N, Aspelund T, Danesh J, Gudnason V. Chronic kidney disease and risk of major cardiovascular disease and

non-vascular mortality: prospective population based cohort study. BMJ 2010;341(sep30 1):c4986.
9. Go AS, Chertow GM, Fan D, McCulloch CE, Hsu CY. Chronic kidney disease and the risks of death, cardiovascular events, and hospitalization. N Engl J Med 2004;351(13):1296–1305.
10. McDonald RJ, McDonald JS, Kallmes DF, et al. Intracranial Gadolinium Deposition after Contrast-enhanced MR Imaging. Radiology 2015;275(3):772–782.
11. Kanda T, Fukusato T, Matsuda M, et al. Gadolinium-based Contrast Agent Accumulates in the Brain Even in Subjects without Severe Renal Dysfunction: Evaluation of Autopsy Brain Specimens with Inductively Coupled Plasma Mass Spectroscopy. Radiology 2015;276(1):228–232.
12. Friedrich MG, Niendorf T, Schulz-Menger J, Gross CM, Dietz R. Blood oxygen level-dependent magnetic resonance imaging in patients with stress-induced angina. Circulation 2003;108(18):2219–2223.
13. Jahnke C, Gebker R, Manka R, Schnackenburg B, Fleck E, Paetsch I. Navigator-gated 3D blood oxygen level-dependent CMR at 3.0-T for detection of stress-induced myocardial ischemic reactions. JACC Cardiovasc Imaging 2010;3(4):375–384.
14. Arnold JR, Karamitsos TD, Bhamra-Ariza P, et al. Myocardial oxygenation in coronary artery disease: insights from blood oxygen level-dependent magnetic resonance imaging at 3 tesla. J Am Coll Cardiol 2012;59(22):1954–1964.
15. Karamitsos TD, Leccisotti L, Arnold JR, et al. Relationship between regional myocardial oxygenation and perfusion in patients with coronary artery disease: insights from cardiovascular magnetic resonance and positron emission tomography. Circ Cardiovasc Imaging 2010;3(1):32–40.
16. Manka R, Paetsch I, Schnackenburg B, Gebker R, Fleck E, Jahnke C. BOLD cardiovascular magnetic resonance at 3.0 tesla in myocardial ischemia. J Cardiovasc Magn Reson 2010;12(1):54.
17. Dharmakumar R, Arumana JM, Tang R, Harris K, Zhang Z, Li D. Assessment of regional myocardial oxygenation changes in the presence of coronary artery stenosis with balanced SSFP imaging at 3.0 T: theory and experimental evaluation in canines. J Magn Reson Imaging 2008;27(5):1037–1045.
18. Ding H, Fernandez-de-Manuel L, Schär M, et al. Three-dimensional whole-heart T2 mapping at 3T. Magn Reson Med 2015;74(3):803–816.
19. Kellman P, Aletras AH, Mancini C, McVeigh ER, Arai AE. T2-prepared SSFP improves diagnostic confidence in edema imaging in acute myocardial infarction compared to turbo spin echo. Magn Reson Med 2007;57(5):891–897.
20. Giri S, Shah S, Xue H, et al. Myocardial T_2 mapping with respiratory navigator and automatic nonrigid motion correction. Magn Reson Med 2012;68(5):1570–1578.
21. Yang HJ, Sharif B, Pang J, et al. Free-breathing, motion-corrected, highly efficient whole heart T2 mapping at 3T with hybrid radial-cartesian trajectory. Magn Reson Med 2016;75(1):126–136.
22. Liu A, Wijesurendra RS, Francis JM, et al. Adenosine Stress and Rest T1 Mapping Can Differentiate Between Ischemic, Infarcted, Remote, and Normal Myocardium Without the Need for Gadolinium Contrast Agents. JACC Cardiovasc Imaging 2016;9(1):27–36.
23. Rongen GA, Brooks SC, Pollard MJ, et al. Effect of adenosine on heart rate variability in humans. Clin Sci (Lond) 1999;96(6):597–604.
24. Bloch F. Nuclear Induction. Phys Rev 1946;70:460.
25. Yang HJ, Yumul R, Tang R, et al. Assessment of myocardial reactivity to controlled hypercapnia with free-breathing T2-prepared cardiac blood oxygen level-dependent MR imaging. Radiology 2014;272(2):397–406.
26. Kumar A, Beohar N, Arumana JM, et al. CMR imaging of edema in myocardial infarction using cine balanced steady-state free precession. JACC Cardiovasc Imaging 2011;4(12):1265–1273.
27. Nakazato R, Berman DS, Dey D, et al. Automated quantitative Rb-82 3D PET/CT myocardial perfusion imaging: normal limits and correlation with invasive coronary angiography. J Nucl Cardiol 2012;19(2):265–276.
28. Slomka PJ. Software approach to merging molecular with anatomic information. J Nucl Med 2004;45(Suppl 1):36S–45S.
29. Bakdash JZ, Marusich LR. Repeated Measures Correlation. Front Psychol 2017;8:456 [Published correction appears in Front Psychol 2019;10:1201.].
30. Zheng J, Wang J, Rowold FE, Gropler RJ, Woodard PK. Relationship of apparent myocardial T2 and oxygenation: towards quantification of myocardial oxygen extraction fraction. J Magn Reson Imaging 2004;20(2):233–241.
31. Vöhringer M, Flewitt JA, Green JD, et al. Oxygenation-sensitive CMR for assessing vasodilator-induced changes of myocardial oxygenation. J Cardiovasc Magn Reson 2010;12(1):20.
32. Dharmakumar R, Hong J, Brittain JH, Plewes DB, Wright GA. Oxygen-sensitive contrast in blood for steady-state free precession imaging. Magn Reson Med 2005;53(3):574–583.
33. Guo H, Au WY, Cheung JS, et al. Myocardial T2 quantitation in patients with iron overload at 3 Tesla. J Magn Reson Imaging 2009;30(2):394–400.
34. Ghugre NR, Ramanan V, Pop M, et al. Myocardial BOLD imaging at 3 T using quantitative T2: application in a myocardial infarct model. Magn Reson Med 2011;66(6):1739–1747.
35. Kellman P, Chefd'hotel C, Lorenz CH, Mancini C, Arai AE, McVeigh ER. High spatial and temporal resolution cardiac cine MRI from retrospective reconstruction of data acquired in real time using motion correction and resorting. Magn Reson Med 2009;62(6):1557–1564.
36. von Knobelsdorff-Brenkenhoff F, Prothmann M, Dieringer MA, et al. Myocardial T1 and T2 mapping at 3 T: reference values, influencing factors and implications. J Cardiovasc Magn Reson 2013;15(1):53.
37. Sharif B, Dharmakumar R, Arsanjani R, et al. Non-ECG-gated myocardial perfusion MRI using continuous magnetization-driven radial sampling. Magn Reson Med 2014;72(6):1620–1628.
38. Marshall HR, Prato FS, Deans L, Théberge J, Thompson RT, Stodilka RZ. Variable lung density consideration in attenuation correction of whole-body PET/MRI. J Nucl Med 2012;53(6):977–984.
39. Vontobel J, Liga R, Possner M, et al. MR-based attenuation correction for cardiac FDG PET on a hybrid PET/MRI scanner: comparison with standard CT attenuation correction. Eur J Nucl Med Mol Imaging 2015;42(10):1574–1580.
40. Nakazato R, Dey D, Alexánderson E, et al. Automatic alignment of myocardial perfusion PET and 64-slice coronary CT angiography on hybrid PET/CT. J Nucl Cardiol 2012;19(3):482–491.